Supplementary Material

Accounting for uncertain 3D elastic structure in fault slip estimates

Théa Ragon[1], **Mark Simons**[1]

[1] Seismological Laboratory, California Institute of Technology, Pasadena, CA, USA.

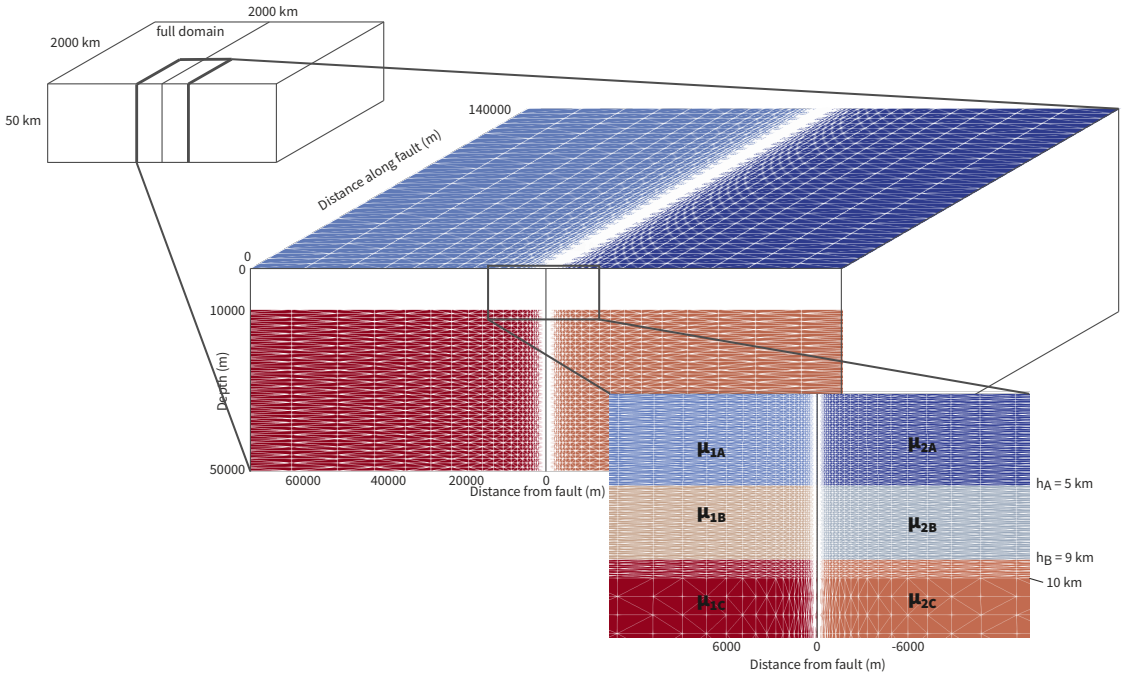

Figure S1 – Illustration of the FEM domain and mesh.

Specification	**Parameter**	**Value**
Geometry	fault	$x = 0$ plane
	h_A	5.0 km
	h_B	9.0 km
Boundaries	x axis	-1000km : 1000km
	y axis	-1000km : 1000km
	z axis	-50km : 0
Boundary Conditions	x positive	zero displacement on every component
	x negative	zero displacement on every component
	y positive	zero displacement on the vertical component
	y negative	zero displacement on the vertical component
	z positive	*no condition imposed*
	z negative	zero displacement on every component
Slip	x axis	NA
	y axis	-250km : 250km
	z axis	-10km : 0
Regions	1A	$-x$ side, above h_A
	1B	$-x$ side, below h_A, above h_B
	1C	$-x$ side, below h_B
	2A	$+x$ side, above h_A
	2B	$+x$ side, below h_A, above h_B
	2C	$+x$ side, below h_B
Number of nodes	along x axis	1003, with a ratio of 0.821 towards fault
	along y axis	33, equally distributed
	along z axis	every 125 m above 10 km
		every 1000 m below 10 km

Table S1 – Grid specifications.

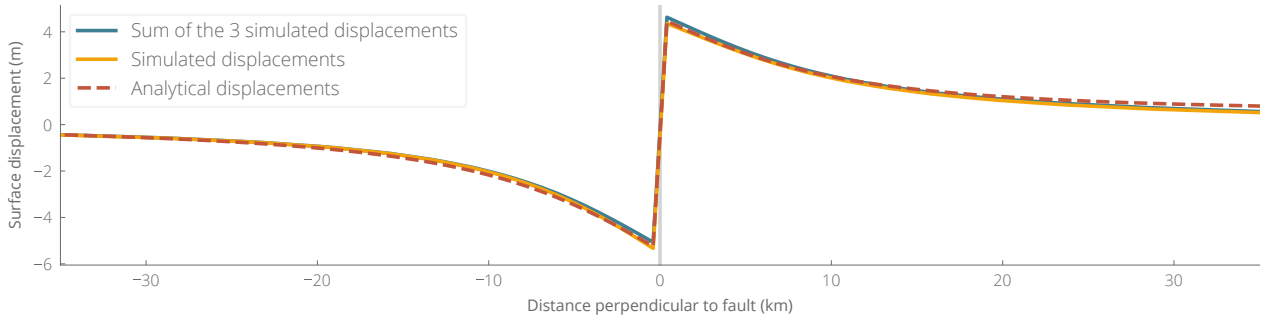

(a) Comparison of analytical or FEM-derived surface displacements. Analytical displacements (dashed red) are approximated from the superposition of 3 similar dislocations in different elastic structures (as explained in Appendix A3. The blue curve has been obtained by summing 3 different FEM simulations corresponding to the 3 different elastic structures. The orange curve corresponds to the displacement simulated with the correct structure (without approximation).

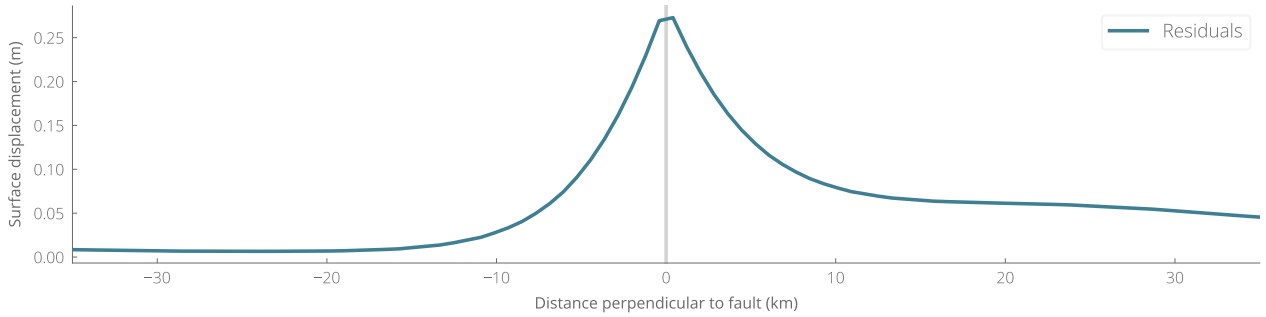

(b) Residuals between the simulated displacement and the approximate analytical solution. The residuals reach a maximum value of 2.5% of the maximum surface displacement.

Figure S2 – Comparison between FEM simulated surface displacements and approximate analytical displacements for an infinite strike slip fault embedded in an elastic structure composed of 2 layers above half space with a lateral heterogeneity (see setup in Fig. A1 and Appendix A4).

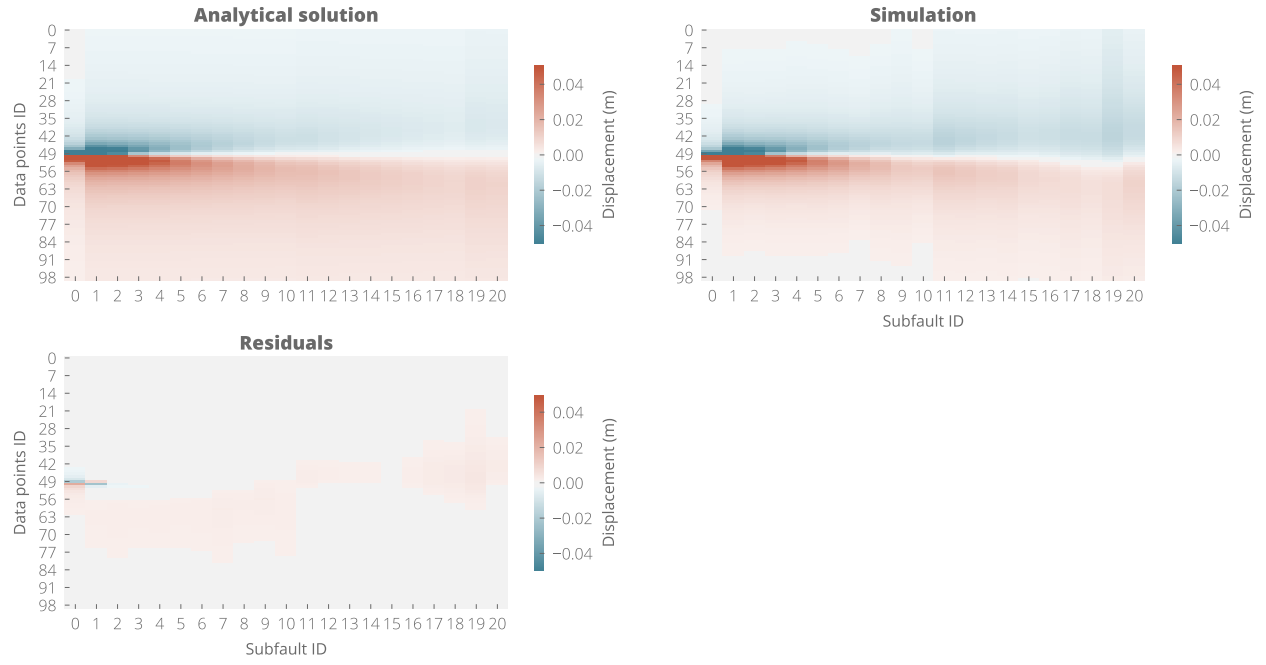

Figure S3 – Comparison of the Green's functions derived from the approximate analytical solution or from a simulation with the domain described in Fig. S1. In this case, the infinite strike slip fault is embedded in an elastic structure composed of 2 layers above half space with a lateral heterogeneity (see setup in Fig. A1 and Appendix A4).

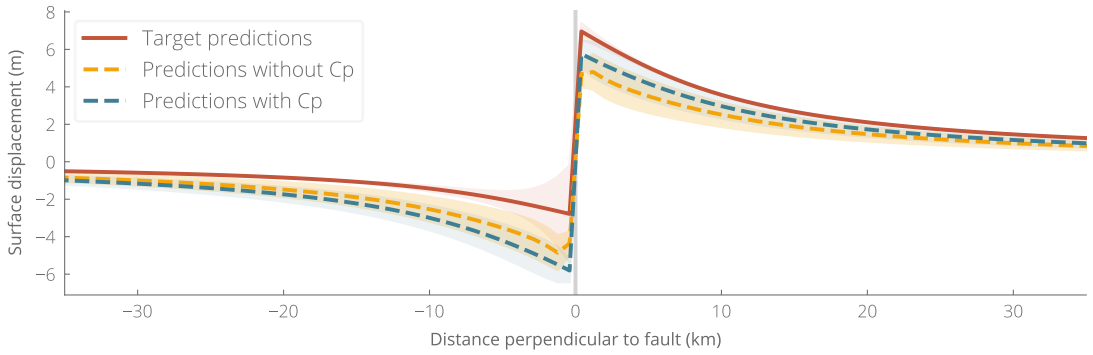

Figure S4 – Comparisons between target predictions (observations) and predictions with and without accounting for $\mathbf{C}_\mathrm{p}$, for an infinite strike slip fault bounding two media of shear moduli μ_1 and μ_2. The target predictions are calculated assuming true Green's functions, while the dashed curves are calculated assuming an homogeneous crustal structure. The uncertainty associated with each curve is in a similar color. The uncertainty of the target predictions contains $\mathbf{C}_\mathrm{p}$. The location of the fault surface rupture is shown with a gray vertical line. The target slip is a uniform slip distribution of 10 m in amplitude.

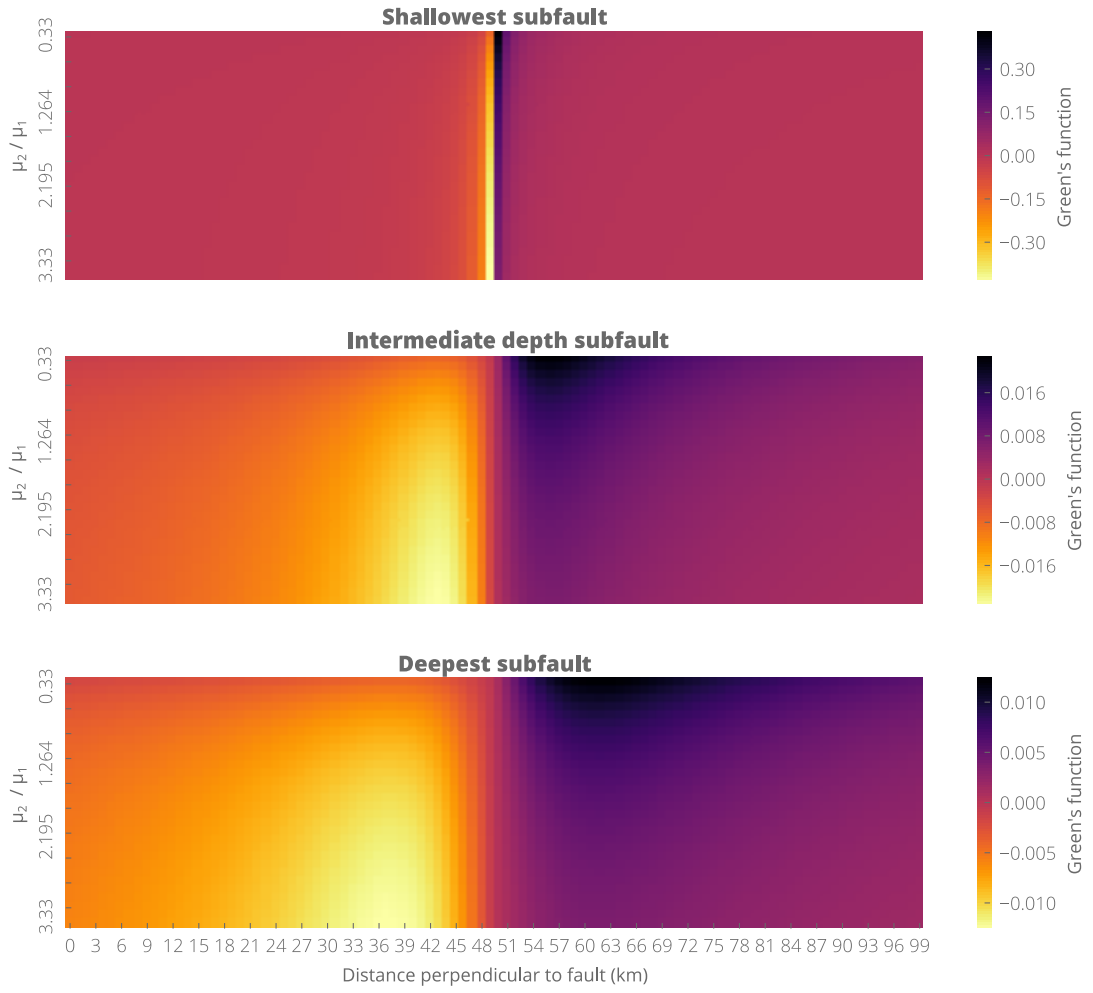

Figure S5 – Variation of the surface displacement (Green's functions) with shear modulus value, for a vertical strike-slip fault bounding two media of shear moduli μ_1 and μ_2. μ_1 (left side of the fault, data from 0 to 50 km) is held fixed and μ_2 (right side) varies. The surface displacement is calculated perpendicularly to the fault (the fault being at 50 km) for a strike slip of 1 m on the shallowest subfault (top), at intermediate depth (middle) or for the deepest subfault (bottom).

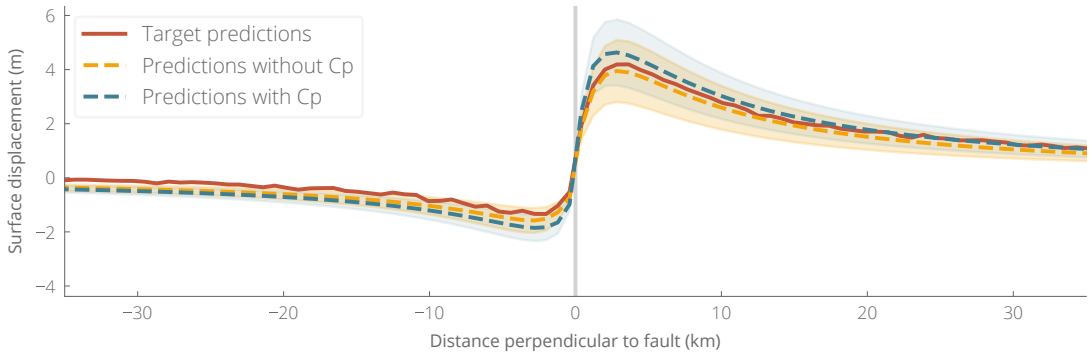

Figure S6 – Same as Fig.S4, but with the target predictions calculated with a non-uniform target slip distribution, and with correlated noise added.

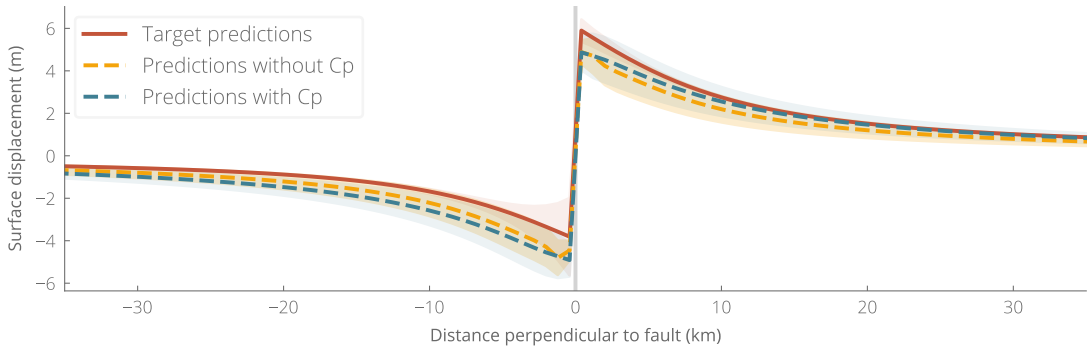

Figure S7 – Comparisons between target predictions (observations) and predictions with and without accounting for $\mathbf{C}_\mathrm{p}$, for an infinite strike slip fault embedded in an heterogeneous media, composed of 2 layers over a half-space and a vertical heterogeneity. The target predictions are calculated assuming true Green's functions, while the dashed curves are calculated assuming an homogeneous crustal structure. The uncertainty associated with each curve is in a similar color. The uncertainty of the target predictions contains $\mathbf{C}_\mathrm{p}$. The location of the fault surface rupture is shown with a gray vertical line. The target slip is a uniform slip distribution of 10 m in amplitude.

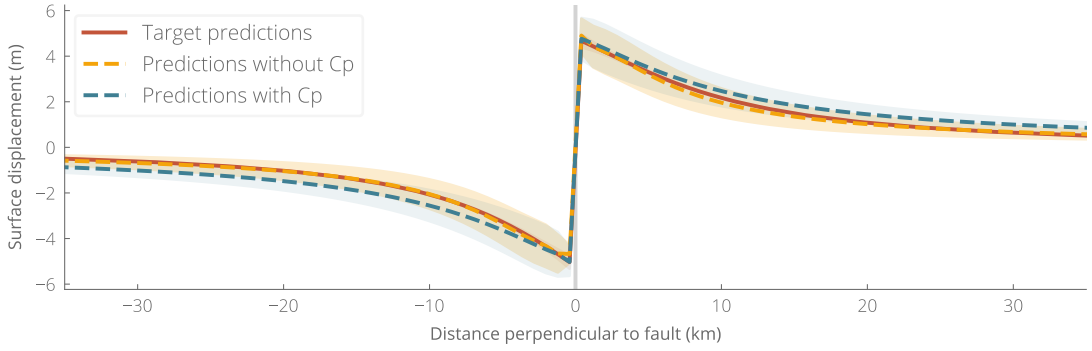

Figure S8 – Comparisons between target predictions (observations) and predictions with and without accounting for $\mathbf{C}_\mathrm{p}$, for an infinite strike slip fault embedded in an heterogeneous media composed of two layers above half space and a vertical heterogeneity, with different velocity gradients on either side of the fault. The target predictions are calculated assuming true Green's functions, while the dashed curves are calculated assuming an homogeneous crustal structure. The uncertainty associated with each curve is in a similar color. The uncertainty of the target predictions contains $\mathbf{C}_\mathrm{p}$. The location of the fault surface rupture is shown with a gray vertical line. The target slip is a uniform slip distribution of 10 m in amplitude.

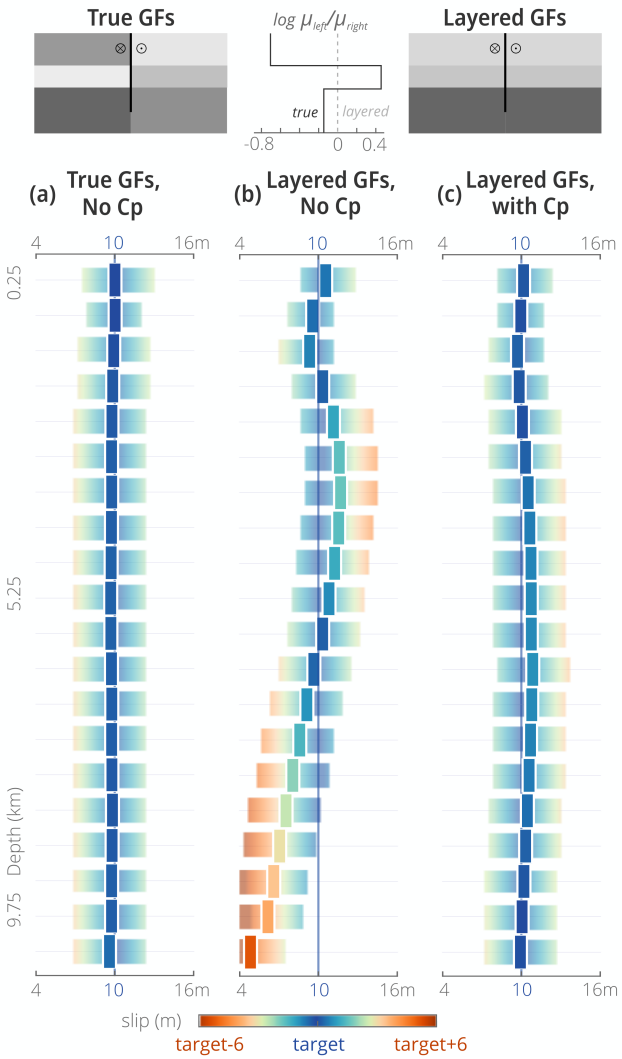

Figure S9 – Same as Fig. 5, with, in (b) and (c), the crustal structure assumed to be layered, and, in (c), epistemic uncertainties calculated by layers and vertical domains. The assumed layered crustal structure is, for each layer, the average of the true structure.

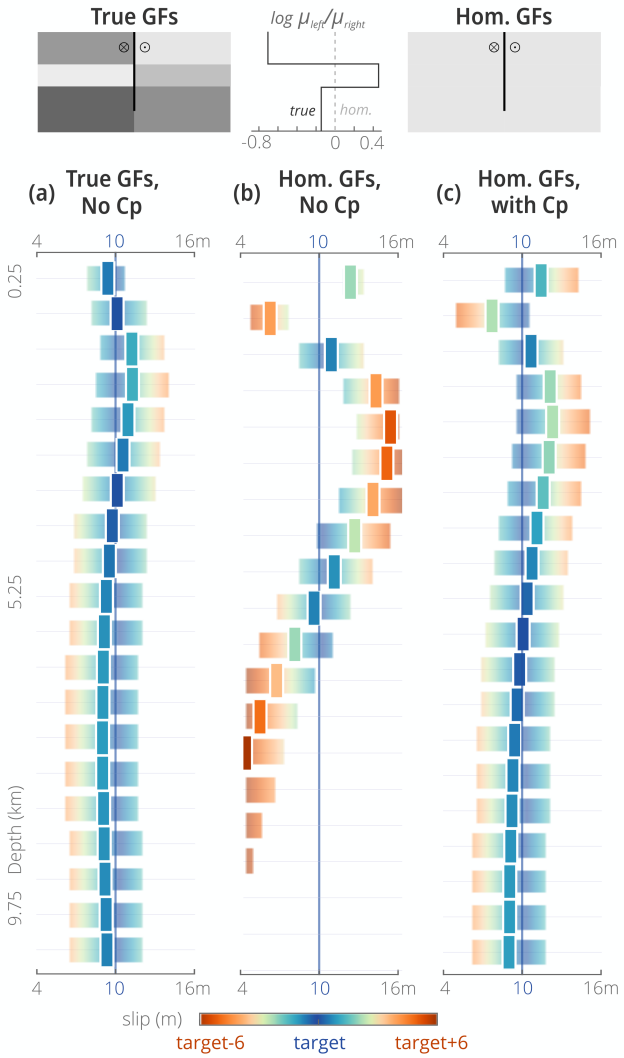

Figure S10 – Same as Fig. 5, with noise added to the synthetic surface displacement. Gaussian noise is combined with spatially correlated noise with a standard deviation being of 6% of the maximum surface displacement.

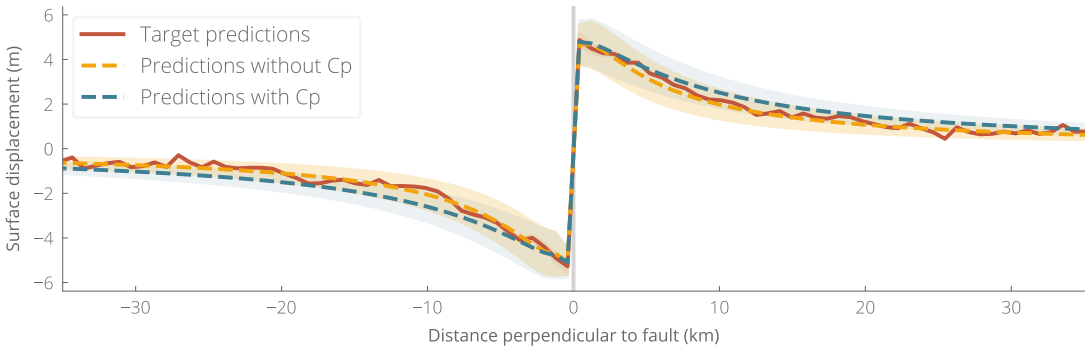

Figure S11 – Same as Fig. S8, with noise added to the synthetic surface displacements (noise realization 1, described in Fig. S10).

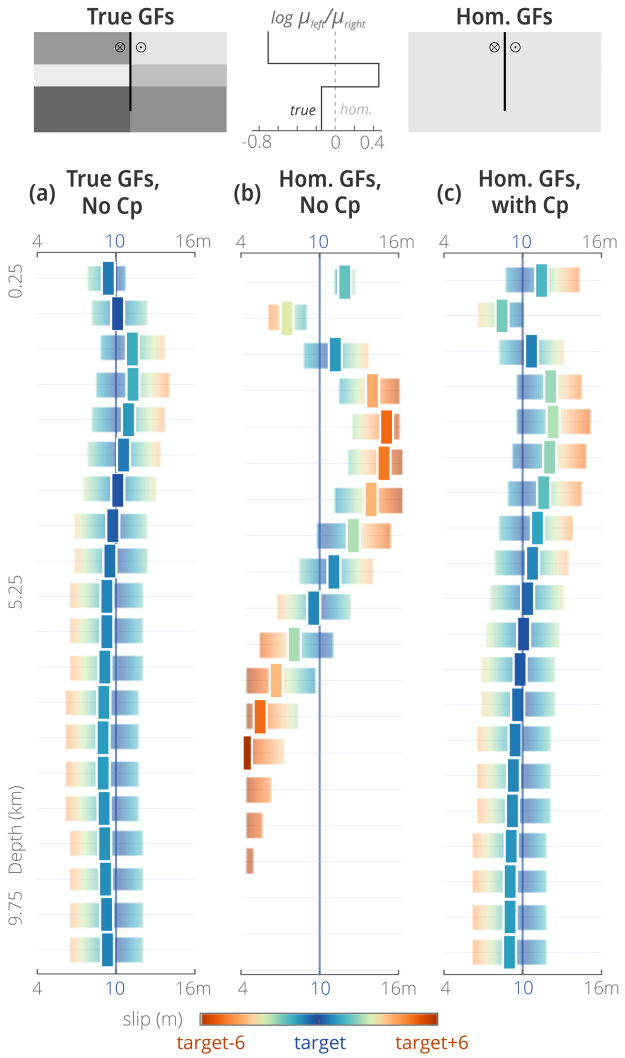

Figure S12 – Same as Fig. 5, with noise added to the synthetic surface displacement. Gaussian noise is combined with spatially correlated noise with a standard deviation being of 9% of the maximum surface displacement.

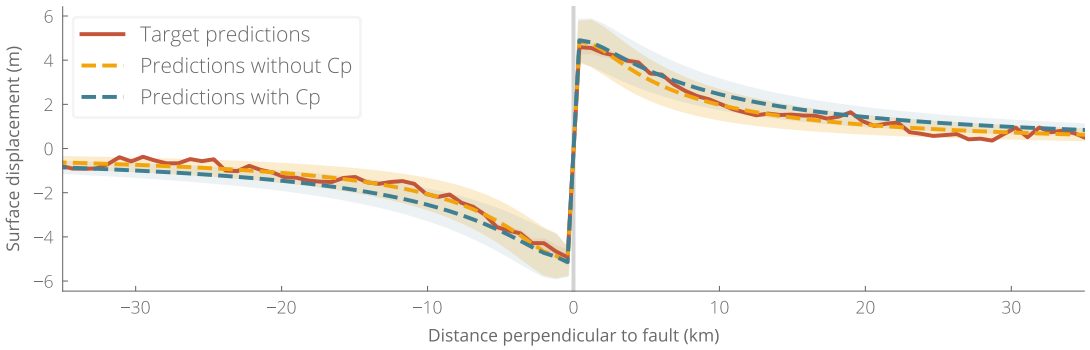

Figure S13 – Same as Fig. S8, with noise added to the synthetic surface displacements (noise realization 2, described in Fig. S12).

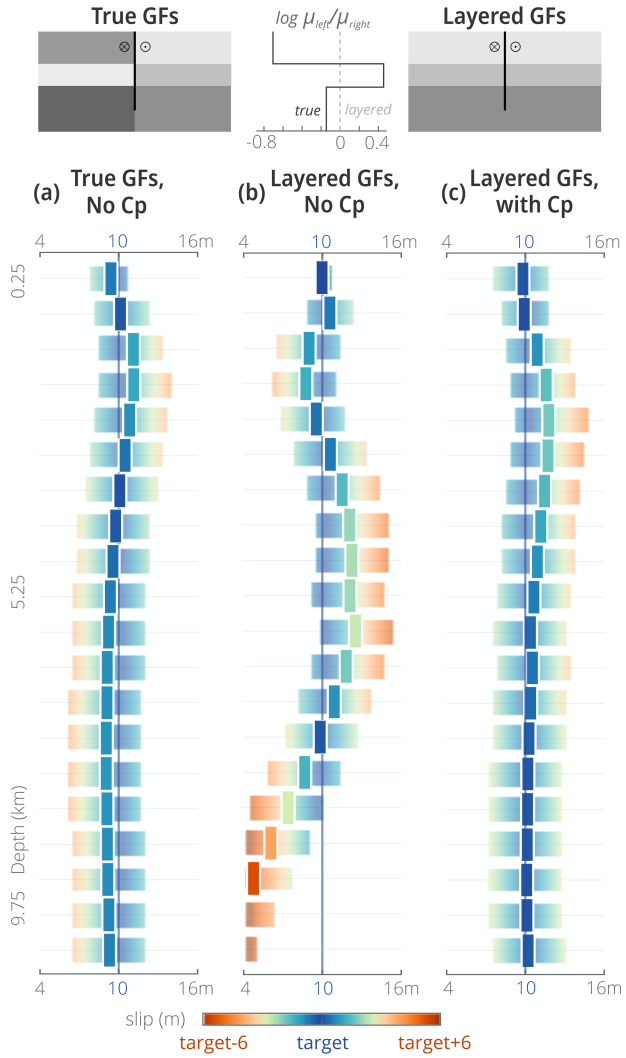

Figure S14 – Same as Fig. 6, with noise added to the synthetic surface displacement, and, in (c) epistemic uncertainties calculated for each domain independently.

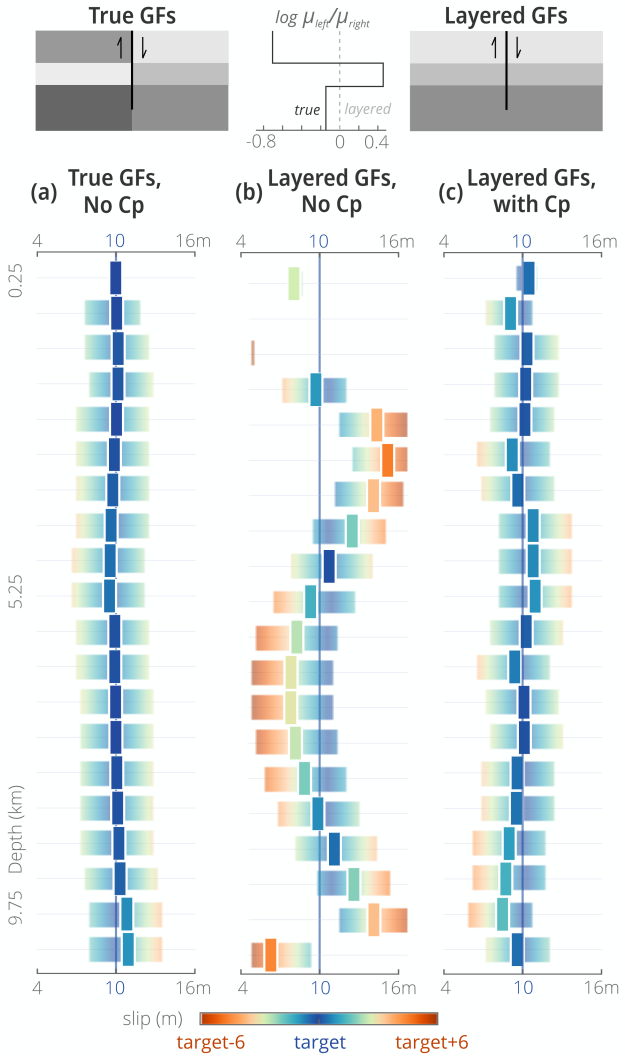

Figure S15 – Same as Fig. 6 but assuming a reverse dip-slip target model. Synthetic surface displacements, Green's functions and uncertainties are FEM-derived.

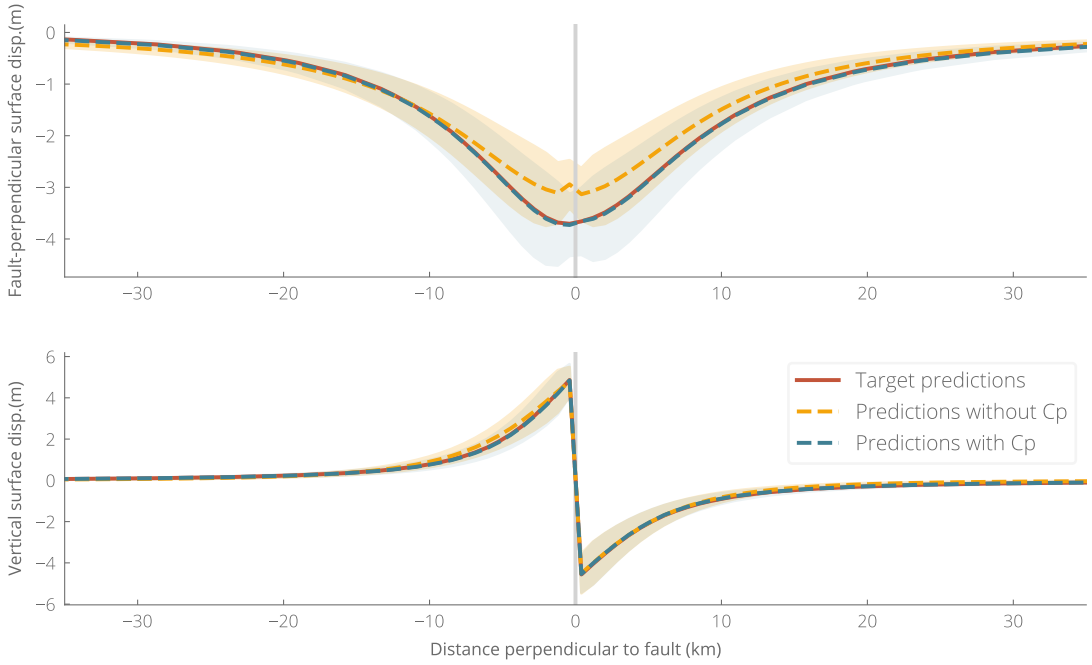

Figure S16 – Comparisons between target predictions (observations) and predictions with and without accounting for $\mathbf{C}_\mathrm{p}$, for an infinite dip slip fault embedded in an heterogeneous media composed of two layers above half space and a vertical heterogeneity, with different velocity gradients on either side of the fault. The target predictions are calculated assuming true Green's functions, while the dashed curves are calculated assuming a layered crustal structure. The uncertainty associated with each curve is in a similar color. The location of the fault surface rupture is shown with a gray vertical line. The target slip is a uniform reverse slip of 10 m in amplitude.

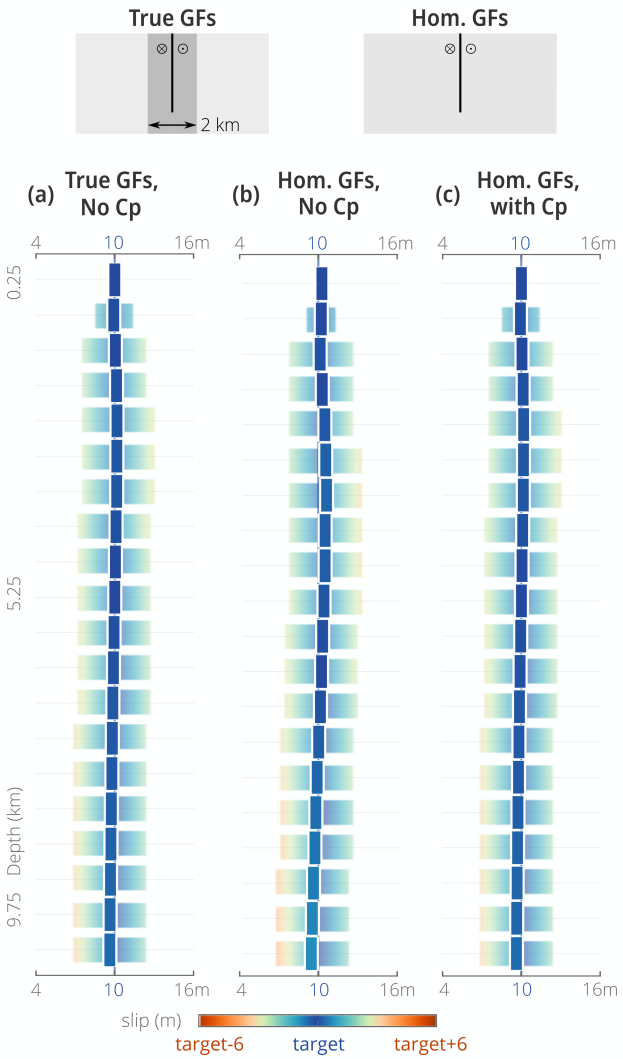

Figure S17 – Same as Fig. 7, with a 2 km wide fault zone.

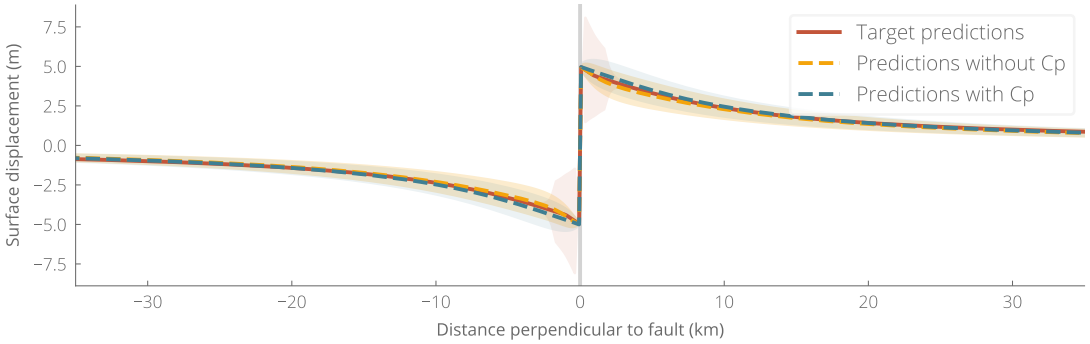

Figure S18 – Comparisons between target predictions (observations) and predictions with and without accounting for $\mathbf{C}_\mathrm{p}$, for an infinite strike slip fault embedded in a compliant fault zone. The target predictions are calculated assuming true Green's functions, while the dashed curves are calculated assuming an homogeneous crustal structure. The uncertainty associated with each curve is in a similar color. The uncertainty of the target predictions contains $\mathbf{C}_\mathrm{p}$. The location of the fault surface rupture is shown with a gray vertical line. The target slip is a uniform slip distribution of 10 m in amplitude.

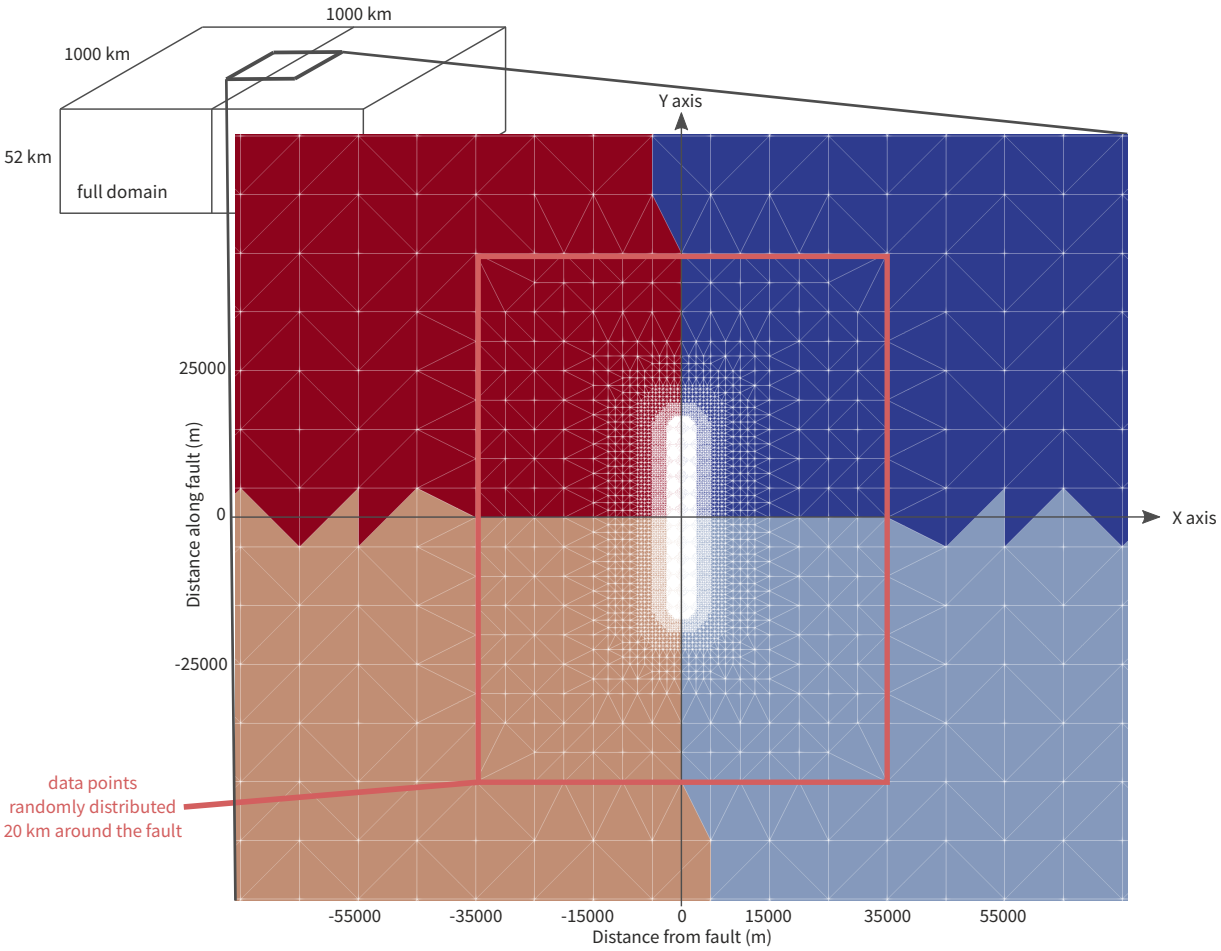

Figure S19 – Illustration of the FEM domain and mesh for the 3D example.

Specification	**Parameter**	**Value**
Geometry	fault	$x = 0$ plane, within $y = [-10km; 10km]$
Boundaries	x axis	-500km : 500km
	y axis	-500km : 500km
	z axis	-52km : 0
Boundary Conditions	x positive	zero displacement on every component
	x negative	zero displacement on every component
	y positive	zero displacement on the vertical component
	y negative	zero displacement on the vertical component
	z positive	*no condition imposed*
	z negative	zero displacement on every component
Slip	x axis	NA
	y axis	refer to Fig. 8(a)
	z axis	refer to Fig. 8(a)
Regions	1	$+x$ and $+y$ quarter
	2	$+x$ and $-y$ quarter
	3	$-x$ and $-y$ quarter
	4	$-x$ and $+y$ quarter
Distance between nodes	along x axis	from 10 km to 150 m 1500 m around the fault
	along y axis	from 10 km to 150 m 1500 m around the fault
	along z axis	from 5 km to 75 m 1500 m around the fault

Table S2 – Grid specifications for the 3D example.

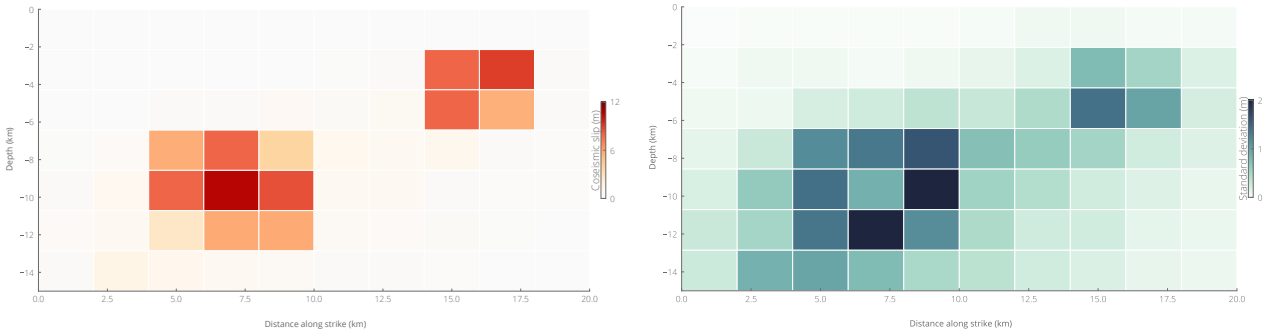

(a) Mean strike-slip amplitude. **(b)** Strike-slip standard deviation.

Figure S20 – Mean model and standard deviation estimated assuming an homogeneous crust, the true crustal structure being homogeneous too.

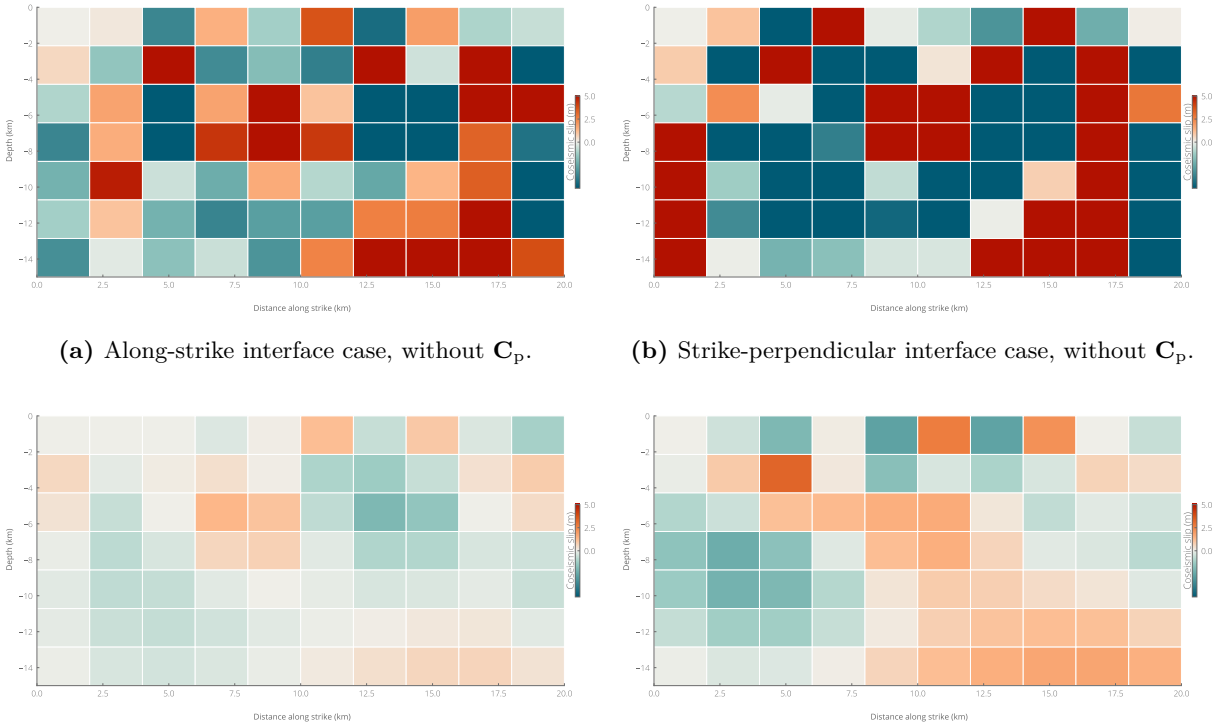

(a) Along-strike interface case, without $\mathbf{C}_\mathrm{p}$. **(b)** Strike-perpendicular interface case, without $\mathbf{C}_\mathrm{p}$.

(c) Along-strike interface case, with $\mathbf{C}_\mathrm{p}$. **(d)** Strike-perpendicular interface case, with $\mathbf{C}_\mathrm{p}$.

Figure S21 – Mean dip-slip amplitude for the cases presented in Fig. 8.

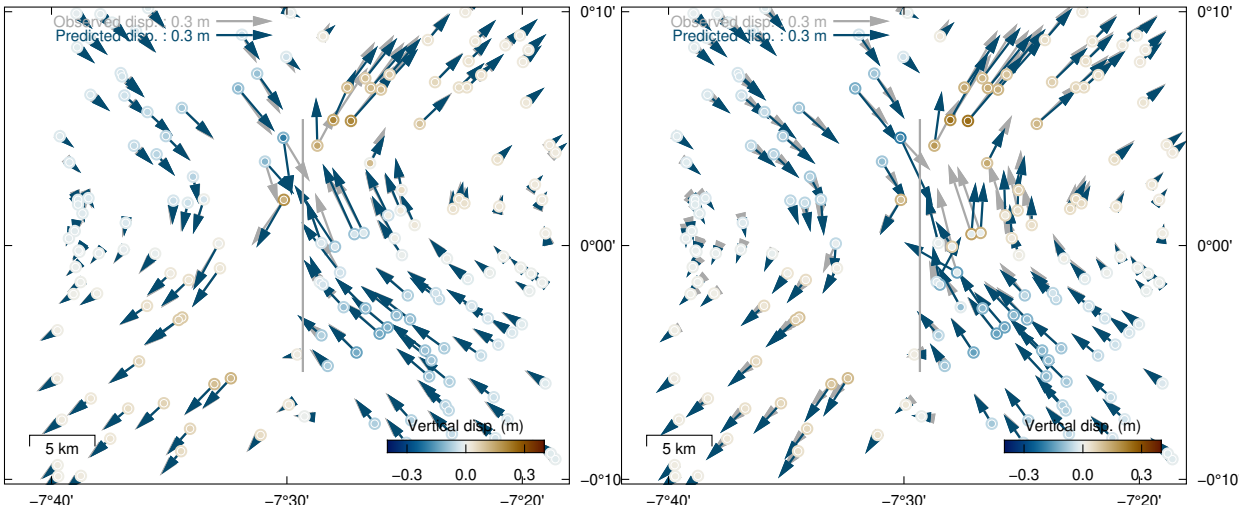

(a) Along-strike interface case, without $\mathbf{C}_\mathrm{p}$.

(b) Strike-perpendicular interface case, without $\mathbf{C}_\mathrm{p}$.

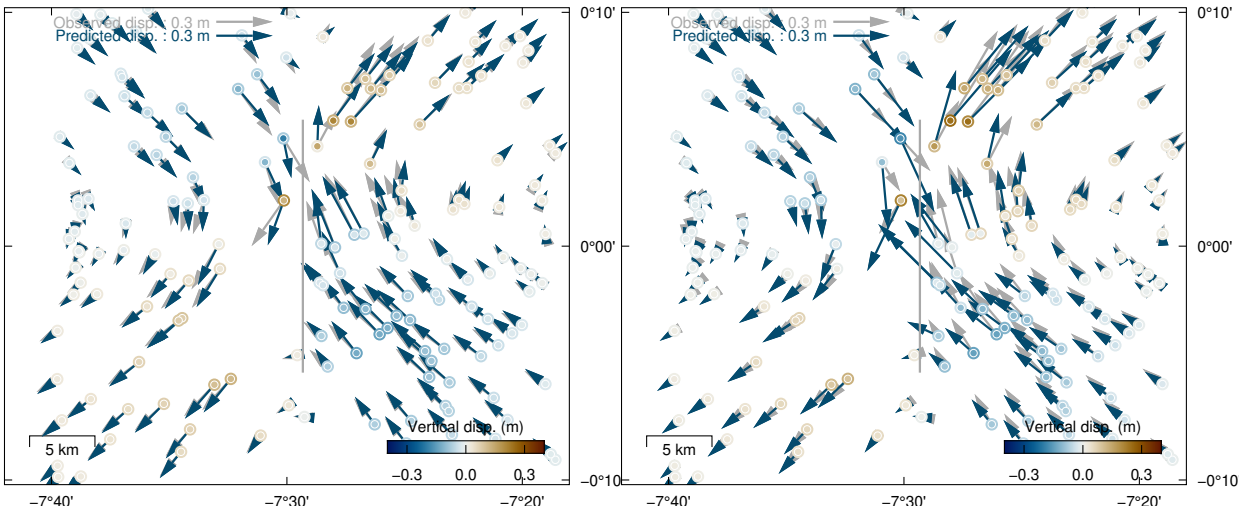

(c) Along-strike interface case, with $\mathbf{C}_\mathrm{p}$.

(d) Strike-perpendicular interface case, with $\mathbf{C}_\mathrm{p}$.

Figure S22 – Comparison between obseved and predicted displacements for the cases presented in Fig. 8. For the vertical surface displacement, the inner values represent the observed amplitudes, and the outer values the predicted amplitudes. The observational and prediction errors are not represented to make the figure easier to read. The average observational error is assumed to be 6% of the displacement. The prediction error depends on whether $\mathbf{C}_\mathrm{p}$ is accounted for or not; it averages at 7% without uncertainties, and 25% with $\mathbf{C}_\mathrm{p}$.

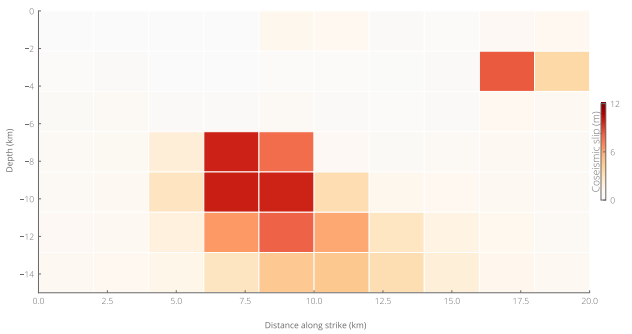

(a) Mean strike-slip amplitude.

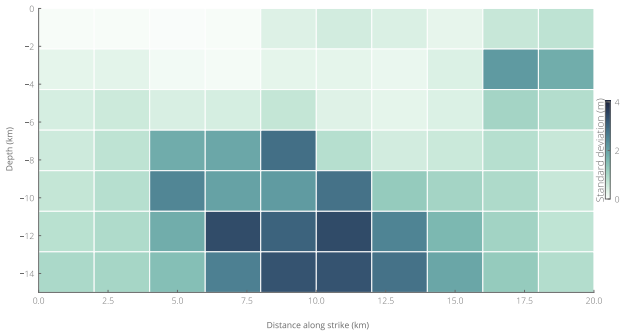

(b) Strike-slip standard deviation.

Figure S23 – Mean model and standard deviation estimated for the strike-perpendicular interface case, without accounting for $\mathbf{C}_\mathrm{p}$, but with a $\mathbf{C}_\mathrm{d}$ proportionally increased so that its amplitude is slightly larger than $\mathbf{C}_\mathrm{p}$. In this case, inferred models are particularly far from the target on the side of the fault which is within the region with a varying shear modulus (right side).